Junctions between CuO_x and ZnO_y in sensors for CO and catalysts for CO hydrogenation

B. J. A. Miller,[a] M. A. Martin-Luengo,[b] M. S. W. Vong,[c] Y. Wang,[d] V. A. Self,[c] S. M. Chapman[c] and P. A. Sermon*[c]

[a]*Central Research Laboratories Ltd, Dawley Road, Hayes, UK UB3 1HH*

[b]*Instituto Rocasolano, C.S.I.C., Calle Serrano 119, 28006 Madrid, Spain*

[c]*Fractal Solids and Surfaces Research Group, Department of Chemistry, Brunel University, Uxbridge, Middx., UK UB8 3PH and Department of Chemistry, University of Surrey, Guildford, Surrey, UK GU2 5XH*

[d]*State Key Laboratory of C_1 Chemical Technology, Department of Chemical Engineering, Tianjin University, Tianjin 300072, P.R. of China*

Addition of CuO_x to defective ZnO_y ($0.92 < y < 1.00$) yielded a dispersed catalyst that produced methanol at 523 K and 2 MPa with a selectivity (relative to CH_4) which was higher than that for a unit area of ZnO_y or CuO_x alone. Copper oxide–zinc oxide polycrystalline films (prepared by ion beam sputter deposition) were as stoichiometric as the dispersed samples with junctions best represented as CuO_x/ZnO_y (with x close to 0.5 and y close to 1.0). Photo-STM reveals for the first time the width and nature of the n/p junction, although the gradient of the depletion zone is shallower on the ZnO side of the junction (which is not expected from recent postulates). Responses to CO and H_2 were more representative of CuO_x than ZnO_y. The properties of such junctions and their role in CO adsorption, catalysis and sensing is discussed, together with the relationship between catalytic and sensor science. Active sites at such junctions may have been detected as those binding CO_2^- with an IR band at 1557 cm^{-1} which decompose to release CO_2 or convert to formyl species (and then methanol) depending upon the prevailing conditions.

Wurtzite ZnO is pyroelectric having opposite polar (0001) and $(000\bar{1})$ faces containing predominantly Zn^{2+} or O^{2-} ions respectively and a non-stoichiometry introduced as an oxygen deficiency, involving interstitial $(Zn^{2+}–2e^-)_i$ pairs and cation and anion vacancies ($\square_M$, $\square_O$). Cu_2O has relatively low density with Cu^+ ions coordinated to only two O^{2-} and has an excess of oxygen.

Between ZnO and Cu_2O semiconductors n/p rectifying junctions occur, across which current is preferentially conducted in one direction. Mobile electrons move from ZnO (and positive holes from Cu_2O) until a potential difference exists which is large enough to prevent further charge transfer, and this defines the junction properties. The concentration of charge defects rises exponentially as an n/p semiconductor junction is approached, and is above a background level at 1.7 μm from the junction.[1] In this depletion zone the electric field has a steeper gradient in the n-type semiconductor and a shallower gradient (*i.e.* the depletion zone extends further) in the p-type semiconductor (*e.g.* Cu_2O).[1] Such a depletion zone is similar in width to the high-resistivity Schottky exhaustion layer[2] at semiconductor surfaces or the depletion layers[3] at Si(111) surfaces in contact with electrolytes seen using optical second harmonic generation.[4]

Semiconductors have long been used for gas sensing.[5] In humidity and CO sensing by ZnO,[6] grain boundaries (detectable by STM[7]) are important,[8] while CuO_x addition to produce Cu_2O/ZnO[5] gives improved sensor selectivity (if not sensitivity) towards CO. Junction chemistry affects performance[9] of such a sensor device, in part because CO can chemisorb across ZnO–CuO interfaces.[10]

Exothermic methanol synthesis ($CO + 2H_2 = CH_3OH$) occurs on industrial catalysts (*i.e.* $Cu/ZnO/Al_2O_3$[11] which contains ZnO and the more readily reduced Cu[12]). It involves CO[13] or CO_2 adsorption (with carbonate formation[14]) on ZnO whose polar surfaces are more active.[11,15] The materials chemistry is complicated by the ease of CuO_x reduction relative to ZnO_y[12] (affecting the concentration of exposed cations and Lewis-acid sites (L), CO adsorption[16] and solid solution[17] or CuO_x/ZnO_y interface formation). It is at these interfaces that active L centres and unique bridging formate species[18–21] may be generated causing a linear relationship between methanol synthesis activity and metallic surface area[19] for related catalysts.

The solid-state and surface properties of CuO_x/ZnO_y junctions are considered in this study in detail with a view to understanding their role in controlling activity and selectivity in CO gas sensing and catalysis of CO hydrogenation. This it is hoped illustrates the relationship between catalysis and gas sensing by solid surfaces more generally.

Experimental

Preparation of dispersed materials

ZnO_y was prepared[18] from an aqueous solution of zinc acetate (BDH; >99.5% purity) by precipitation with NaOH–$NaHCO_3$ (BDH; AnalaR) at a final pH of 9–10. This was washed well with distilled water to constant filtrate conductivity, dried in air at 403 K and calcined in air at 523 K for 3 h. CuO_x/ZnO_y with a Cu concentration corresponding to 8 mass% was prepared[22] in a similar manner in the presence of copper(II) nitrate; its composition was expected to maximise the potential for junction formation. During precipitation CuO_x and ZnO_y phases appeared simultaneously as the pH rose (thereby presumably enhancing further the probability of junction formation). Both exhibited the same ZnO X-ray structure after calcination.

Preparation of polycrystalline films

ZnO has been grown upon Cu(110), as have Cu overlayers upon ZnO.[23] Here Cu and Zn (99.99% purity; Goodfellows Metals) were used to prepare ZnO layers upon Cu_2O (with a well defined junction between these) by argon atom beam-sputter deposition in an argon(0.6 Pa)–oxygen(0.4 Pa) atmosphere. Au-coated glass (pre-washed with acetone and then deionised water, dried at 393 K, and evacuated to <0.2 Pa, and pre-coated with Ni–Cr/Au) was used as the substrate.

Cu_2O was first applied, followed (after chemical masking of half of the Cu_2O) by ZnO in a manner similar to that already described.[9]

Characterisation methods for dispersed samples

Total surface areas were estimated by BET analysis of N_2 adsorption at 77 K. Temperature-programmed reduction (TPR) was followed in flowing 5%H_2–Ar on heating at 10 K min^{-1}. Solid-state conductivities in the ZnO_y were measured in flowing N_2 as in ref. 24. The extent of adsorption of CO, H_2 and CO_2 at 298 K was measured volumetrically after *in-situ* reduction at 523 K and outgassing. The first and last of these are inter-related in that CO_2^- is seen as an intermediate following CO adsorption on ZnO[25] and CO_2 is often thought to raise x in CuO_x in such catalysts. FTIR was applied to the CuO_x/ZnO_y samples during CO adsorption at 298 K and 6.08 kPa and desorption (into flowing N_2) using a Perkin Elmer 1710 FTIR spectrometer. X-Ray photoelectron spectroscopy (XPS) and electron paramagnetic resonance were carried out in Kratos E300 and Varian E3 instruments. Cu-Kα radiation (Ni-filtered; 20 kV and 30 mA) was used to ascertain the structure of the crystalline components in pre-calcined samples. Activities of samples (0.1 g) held in an inert glass-lined stainless-steel reactor in CO hydrogenation were measured after *in-situ* reduction in 6%H_2–N_2 during heating from 298 to 573 K (where they were held for 30 min before cooling to 523 K). Conversions were followed at 2 MPa and 523 K in a reactant stream of H_2–CO (1:2 or 2:1) flowing at 16 cm^3 min^{-1} with analyses as a function of time conducted as previously.[22] Activity of the reactor system alone was negligible and streams were cleansed of metal carbonyls.

Characterisation methods for polycrystalline films

DC current–voltage characteristics were analysed at 298 K in dry flowing N_2 (oxygen-free; BOC), and nitrogen containing 0.2% CO (BOC) or 6% H_2 (BOC). XPS of films was undertaken within an Escalab 210 (calibrated with C ls at 284.6 eV). STM has been used previously[26] to study ZnO single crystals, ZnO/liquid interfaces and TiO_x overlayers upon metals. In this work moderate resolution AFM/photo-STM images were obtained (Park Scientific Autoprobe). With the latter technique irradiation of the film was achieved with a wide band visible source (Fiber-Lite Model 190 fiber optic illuminator (Dolan-Jenner Industries Inc, Woburn, MA), which it was expected would facilitate electron tunnelling. The surface texture and the chemical nature (*e.g.* the Zn concentration) of the interface region were examined by scanning electron microscopy (JEOL JXA 840A). Pyridine adsorption on the film junction at 298 K for 12 days was analysed by *in-situ* micro-FTIR[27] in a reflectance mode after flushing in flowing N_2 at 298–455 K.

Results for dispersed samples

The ZnO_y (32 m^2 g^{-1}) and CuO_x/ZnO_y (66 m^2 g^{-1}) were, after calcination, crystalline in an X-ray diffraction (XRD) sense. The resistivity[28] of the uncalcined dispersed ZnO_y in N_2 (Fig. 1) during four successive thermal cycles increased with increasing temperature (and exhibited hysteresis). At *ca.* 723 K its resistivity appeared to rapidly diminish as a result of annealing which removed defects inherited from the precursor hydrozincite→ZnO transformation. Other evidence of non-stoichiometry came from the EPR signal [$g = 1.9335$; see insert to Fig. 1(*a*)] at 298 K, that was close to that seen for ZnO[30] at 97–470 K, which decreased in intensity on oxygen chemisorption at 298 K.[31] Such non-stoichiometry is presumably related to the presence of exposed cation Lewis (L)-acid sites.[18]

During CO adsorption or catalysis of CO hydrogenation any non-stoichiometry will be enhanced (given the reducing power of CO[29]). ZnO_y reduced in TPR with a maximum rate

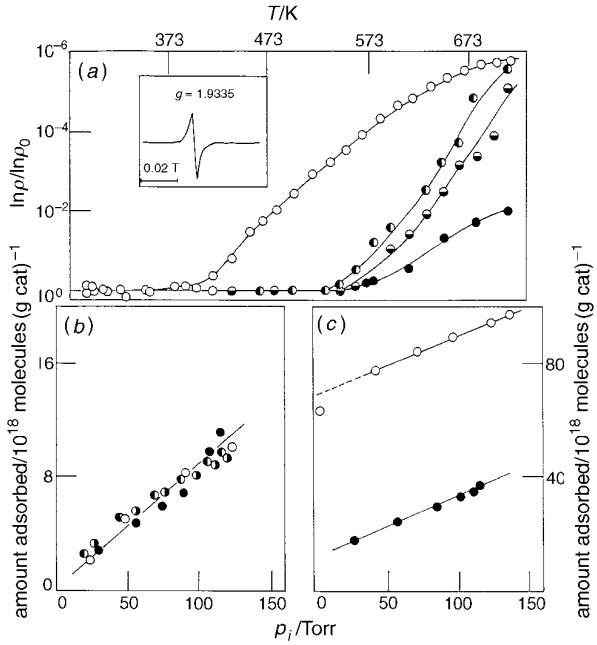

Fig. 1 (*a*) Relative resistivity of ZnO in N_2 as its temperature is raised during first (○), second (◐), third (◒) and fourth (●) thermal cycles, suggesting the removal of vacancies and interstitials during 'annealing' at the higher temperatures. Inset is the EPR signal seen for the as-produced ZnO. (*b*) Adsorption isotherms for H_2 (○, ●) and CO (◐, ◑) and (*c*) CO_2 (○ ●) on ZnO at 298 K. Filled symbols and ◑ denote reversibly held species which for CO_2 are a smaller fraction of the total uptake than for CO or H_2. (1 Torr = 133 Pa)

at 763 K, even though this was limited to a modest uptake (85 μmol H_2 g^{-1}), corresponding to the formation at 523 K of $ZnO_{0.92<y<1.00}$. This was also suggested by *in-situ* XPS, where ZnO reduced at 573 K in 6 kPa H_2 had its Zn $2p_{3/2}$ binding energy decreased by 1.4 eV. The hydrogen uptake in TPR was much larger (2170 μmol g^{-1}) for 8%CuO_x/ZnO_y ($x \leqslant y$), although ZnO neither enhances nor retards CuO_x reduction, nor does it stabilise intermediate crystalline Cu_2O formation.[30]

The weakness of the adsorption of CO and H_2 by ZnO_y is illustrated in Fig. 1(*b*) in terms of uptakes at zero pressure intercepts and isotherm reversibility. CO_2 [Fig. 1(*c*)] on the other hand is adsorbed more strongly and extensively. Each 10–20 nm^2 of the ZnO_y surface was merely capable of adsorbing at L sites about two H or one CO, but this concentration could increase under catalytic conditions (523 K and 2 mPa)[32] with an uncertainty concerning the number of sites active in this reaction.[33] For CuO_x/ZnO_y there was a higher adsorbate concentration (*i.e.* 46.4×10^{18} H atoms g^{-1} or 25.6×10^{18} CO molecules g^{-1}; corresponding on average to one adsorbate molecule per 3 nm^2). IR of pyridine adsorption can probe L sites (at 1440 cm^{-1}) and B acid sites[18] (see Fig. 2). A peak at 1590 cm^{-1} is for non-specifically H-bonded pyridine, but is lost on CuO_x addition.[34] Such IR[35] sees predominantly non-junction species, but Bailie *et al.*[21] have considered CO adsorbed at 295 K and 26.6 kPa on Cu/silica with varying levels of ZnO addition. As the ZnO content increased, they found the band for CO on Cu^{x+} at 2115 cm^{-1} (seen in addition to a shoulder at 2070 cm^{-1} for linearly adsorbed CO on Cu^0) decreased in intensity, but a band at about 2180 cm^{-1} increased in intensity. This may well be the CO interacting with junction sites. Fig. 3 explores this matter further using IR analysis of the 8%CuO_x/ZnO_y during N_2 flushing after adsorbing CO at 298 K. This flushing was designed to remove gaseous and weakly adsorbed (or spectator) CO. The assignment of the relevant bands suggests that with flushing: (*a*) there is rapid loss of linearly bound CO (a or i) (2100 cm^{-1}), but that the

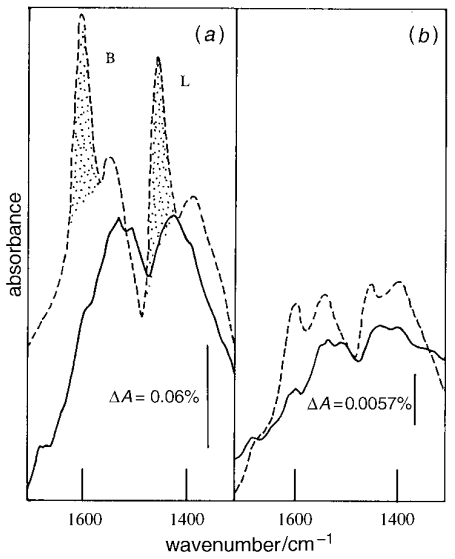

Fig. 2 IR reflectance spectra (scale denotes % change in absorbance) for ZnO_y (*a*) and CuO_x/ZnO_y (*b*) before (—) and after (– – –) pyridine adsorption. L and B denote pyridine adsorbed on Lewis and Brønsted acid sites, whose absorption bands are shaded.

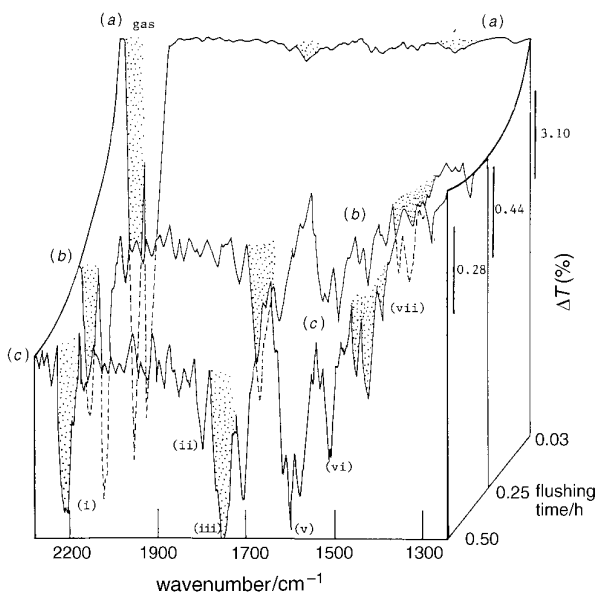

Fig. 3 FTIR spectra of 8% CuO_x/ZnO_y after CO adsorption at 298 K (6.08 kPa) and N_2 flushing for 0.03 h (*a*), 0.25 h (*b*) and 0.5 h (*c*) where the following assignments are made: (i) linearly bound CO revealed after removal of gaseous CO (2100–2170 cm^{-1}); (ii) formate species (1720–1740 cm^{-1}); (iii) carbonyl stretch for formate species (1700 cm^{-1}); (iv) water bending vibration (1645 cm^{-1}); (v) CO_2^- stretch (1557 cm^{-1}); (vi) unidentate carbonate (1393–1455 cm^{-1}); (vii) CO stretch for formate species. The feature at 1557 cm^{-1} is especially interesting.

species (b) at 2170 cm^{-1} remained on the surface to a greater extent; (*b*) there are increasing fractions of formate species (ii) (1720–1740 cm^{-1}), formate species (iii) (carbonyl stretch at 1700 cm^{-1}), water (iv) bending vibration at (1645 cm^{-1}), CO_2^- (v) (stretch at 1557 cm^{-1}), unidentate carbonate (vi) (1393–1455 cm^{-1}) and formate species (vii) (CO stretch).

It would be reasonable to suppose that linearly bound CO [species (a)] is lost, while more strongly bound (b) species participate in the catalysis and sensor chemistry (in part at the junction). The CO_2^- species seen at 1557 cm^{-1} is especially interesting in the light of the report that CO_2^- is formed as an intermediate on ZnO (0001) during CO adsorption.[25]

Table 1 gives the rates of alkane and alcohol production during the hydrogenation of CO at 523 K and 2 MPa over dispersed ZnO_y and CuO_x/ZnO_y. Activities and selectivities towards methanol increased with reaction time significantly,[22] in parallel to increasing levels of surface reduction. The rates of formation of methanol molecules per CO adsorption site h^{-1} (or turnover number, TON) are modest compared with the rates of reactant–surface collision, but are for CuO_x/ZnO_y almost 13 times higher than for ZnO_y.

Fig. 4 considers the effect on selectivity to methanol over methane of Cu dispersion [deduced from N_2O decomposition or CO adsorption (assuming that there are 1.47×10^{19} Cu atoms m^{-2})[22,36]]. This selectivity (*i*) is time-dependent (as shown by the arrows for two samples in this figure),[22] (*ii*) increases as the Cu dispersion increases and (*iii*) increases

Table 1 Rates *r* of formation of various alkanes and alcohols from $CO–H_2$ (1:2) at 2 MPa, 523 K and a flow rate of 16 cm^3 min^{-1} over ZnO_y

	r/nmol (g cat min)$^{-1}$						
	alkanes			alcohols		TON CH_3OH/h	
t/min	C_1	C_2	C_3	C_1	C_2	ZnO_y	CuO_x/ZnO_y
45	29	8	2	390	0	4.39	55.18[a]
90	31	12	8	1530	10	17.21	
135	30	8	7	1430	14	16.09	
175	25	7	2	1870	14	21.04	
220	30	6	2	1980	14	22.28	

[a]At $CO–H_2 = 2:1$ and 15 cm^3 min^{-1}.

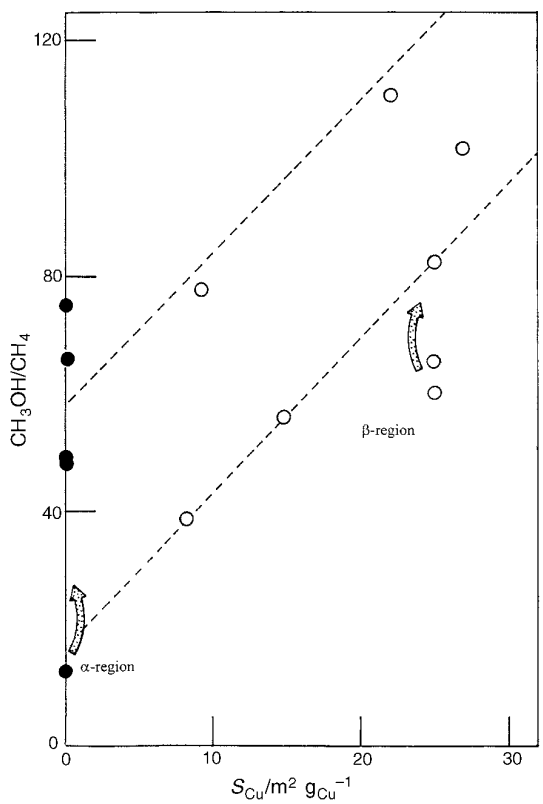

Fig. 4 Effect of Cu dispersion on the selectivity of Cu/ZnO (○) and ZnO_y (●) samples during CO hydrogenation at 523 K, 2 MPa, $CO:H_2 = 2:1$ MPa using present and previous[22] data. Arrows indicate that for any sample CH_3OH/CH_4 product ratios increase with time of use.

as CuO_x is added to ZnO_y. This last additional selectivity is not caused by Cu alone, because neither titania- nor silica-supported CuO_x samples show the same selectivity.[22] In Fig. 4 the selectivity intercept (α) could be attributed to the inherent properties of the ZnO_y and gradient β to the additional selectivity provided by CuO_x/ZnO_y interfaces. It is relevant to ask whether there could be transformation[37] of the 1557 cm^{-1} species to formyl species, with Zn—H generated by dissociative heterolytic H_2 adsorption on ZnO (with bands at 840 and 810 cm^{-1} [38]), but as yet there is no way of separating out and understanding the microchemistry at these interfaces in dispersed samples.

Results for polycrystalline films

Cu/ZnO films and single crystals are used as model methanol synthesis catalysts[39] and have interfacial regions which may be easier to analyse than in dispersed samples; they also act as model sensors.

Scanning electron microscopy and microprobe analysis of the present film showed [Fig. 5(*a*)] that each component was texturally smooth, with a constant concentration of Cu across the sample, even below the electron-transparent zinc oxide top coat, but zinc from the oxide top-coat (where it exists) had a constant concentration only on one side of the junction, beyond which it decreased and could only be detected up to 5 μm beyond the junction (presumably reflecting the efficiency of masking).

The voltage–current characteristics of this junction [Fig. 5(*b*)] did not suggest true rectification, but showed negligible hysteresis. Photoelectron spectra [Fig. 5(*c*),(*d*)] yielded binding energies for 2p states of 1021.0 eV for Zn $2p_{3/2}$ (close to that for Zn^{2+})[40] and 932.2 eV for Cu $2p_{3/2}$ (close to that for Cu^+) suggesting that the film junction (arrowed) was between Cu_2O and ZnO.

Fig. 6 shows the increasing resistance observed at constant voltage when low partial pressures of CO (2000 ppm) or H_2 (6%) were introduced in flowing nitrogen at 295 K. These reductants will increase the concentration of oxygen vacancies $\square_O$ in ZnO, and decrease the oxygen excess in Cu_2O. The responses here are reasonably fast given the modest temperature of operation, but are more typical of the p-type Cu_2O than the ZnO. The film is clearly more sensitive to the better reductant CO, but appeared to respond irreversibly at this low temperature.

Junction chemistry, not accessible in dispersed samples, may be investigated in the polycrystalline films (*e.g.* Fig. 7 gives micro-FTIR evidence of the nature and extent of pyridine adsorption at the ZnO/Cu_2O junction and on either side of it). Spectra for the surface of the ZnO surface and the ZnO/Cu_2O interface indicate the presence of physically adsorbed pyridine (1434 cm^{-1}) and pyridine adsorbed on L acid sites (1453, 1489 and 1574 cm^{-1}) and B acid sites (1489, 1555 and 1638 cm^{-1}) and hydrogen-bonded pyridine (at 1489 and 1607 cm^{-1}). Observation of pyridine on L acid sites means that the ZnO film so formed is non-stoichiometric like the dispersed ZnO_y sample. As the sample was evacuated at increasing temperature (313, 384 and 455 K), the intensity of the vibration bands due to the L acid sites diminished while the bands related to the B acid sites remained relatively

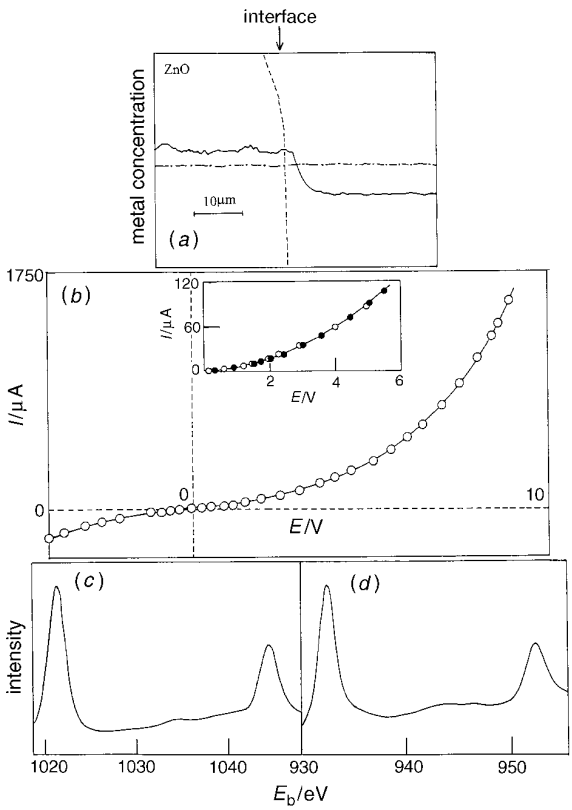

Fig. 5 (*a*) Microprobe analysis for Zn (—) and Cu (–·–) at a ZnO/Cu_2O interface (---) in a film whose position is marked vertically. (*b*) Current–voltage characteristics for the junction in Fig. 5(*a*) (and inset the reversibility of such data where filled symbols denote data with increasing *I*) at 295 K. Photoelectron spectra for the ZnO (*c*) and the Cu_2O (*d*) components of the film in Fig. 5(*a*).

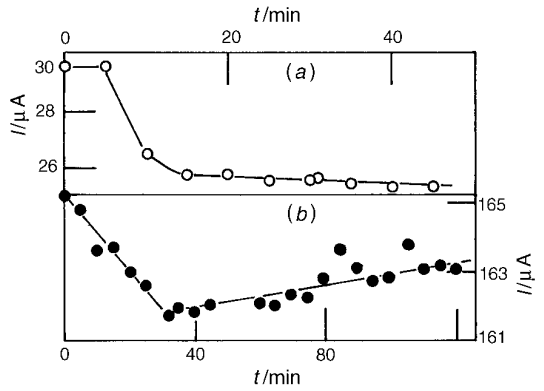

Fig. 6 Time dependence of the response of the ZnO/Cu_2O junction in the film shown in Fig. 5(*a*) to 0.2% CO (*a*) and 6.0% H_2 (*b*) in flowing N_2 at 295 K. CO and H_2 were introduced at $t=0$ min.

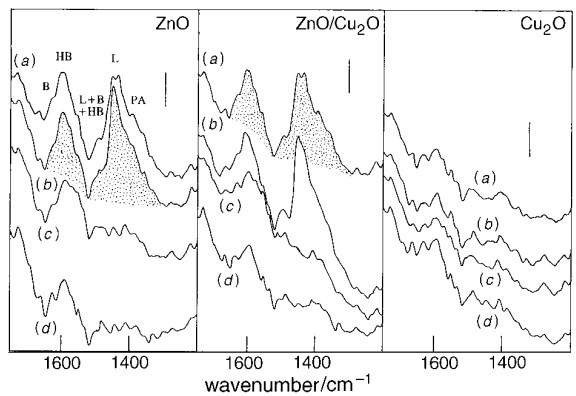

Fig. 7 Micro-FTIR reflectance spectra of pyridine adsorbed on Brønsted acid sites (B), Lewis-acid sites (L) or physically adsorbed (PA) or hydrogen-bonded (HB) onto the ZnO, the ZnO/Cu_2O junction and the Cu_2O components of the film shown in Fig. 5(*a*) at 295 K and then desorbed for 0.25 h into flowing N_2 at (*a*) 295 K, (*b*) 313 K, (*c*) 384 K and (*d*) 455 K. Shaded peaks relate to surface-held pyridine. (Vertical scale bars: $\triangle A=0.03\%$).

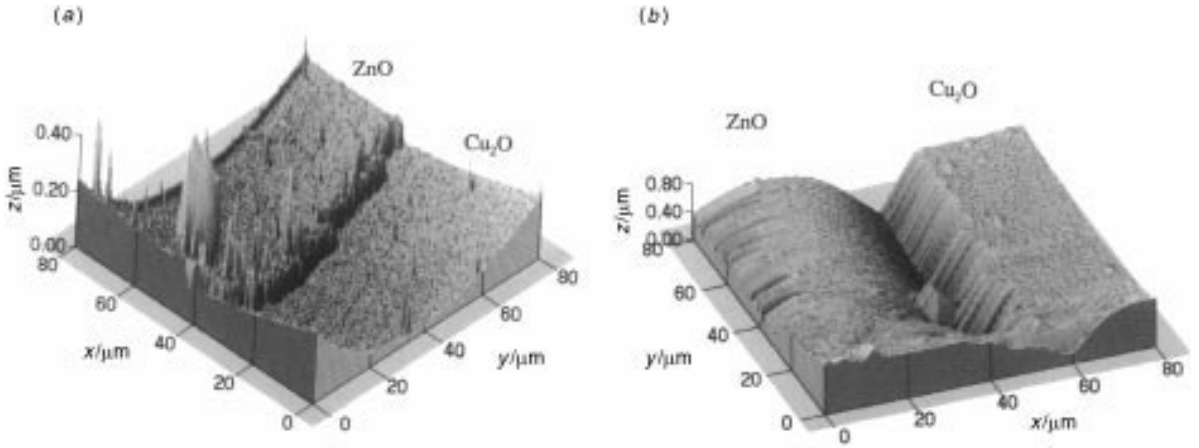

Fig. 8 Moderate resolution AFM (*a*) and photo-STM (*b*) of a ZnO/Cu_2O junction in the film shown in Fig. 5(*a*)

unchanged. It is important to note that no pyridine apparently adsorbed on the surface of Cu_2O. ZnO_y may be partially masking the junction, since CuO_x/ZnO_y does not adsorb pyridine in the dispersed state [Fig. 2(*b*)] but does in Fig. 7. There is NEXAFS evidence[41] that at 295 K pyridine sits upright on a $(10\bar{1}0)$ surface of ZnO (acting as an electron donor[42]) and the L concentration at the film junction could be higher producing the pyridine adsorption seen in Fig. 7 because the fraction of $(10\bar{1}0)$ orientations was higher (less random) than in the dispersed phase or alternatively at the film interface (along the boundary line between ZnO_y and CuO_x) there could be steric hinderance relating to the α-C—H/substrate interactions. It remains difficult to say from micro-FTIR that pyridine is adsorbed at the film junction and this will remain unsolved until the spatial resolution of the micro-FTIR at present improves using higher intensity photon sources.

AFM at modest resolution indicates (Fig. 8) that the ZnO/Cu_2O junction was quite sharp with a 'step' of some 100 nm in height on moving from the ZnO top-coat to the Cu_2O underlayer. This is the physical size of the step at the ZnO/Cu_2O interface in the polycrystalline film measured by AFM. However, photo-STM suggested that a 3–4 μm wide electron valley exists at the interface (although, it is important to remember that microprobe analysis [Fig. 5(*a*)] indicates that Zn extends 5 μm out beyond the formal interface in decreasing concentration).

Discussion

The introduction of CuO_x/ZnO_y interfaces and junctions may alter the number of L sites in ZnO_y and generate sites for enhanced CO adsorption and selective methanol synthesis.[43] Such an example of the synergy between the Zn and Cu components[44] may involve Cu_2O building blocks being inserted into an O vacancy and removing a L acid site at the same time in the ZnO_y. This would cause the formation of a non-symmetrical Zn—O—Cu linkage which could interact uniquely with CO.

Schottky[45] suggested that when ZnO was in contact with a metal its conduction and valence bands rose by 0.5 eV as the junction was approached.[46] Not only will the junction chemistry affect reactant adsorption, but CO (and to a lesser extent H_2) will conversely also have an effect upon the charge flow at the n/p ZnO/Cu_2O junctions. Cu_2O obviously reacts more easily with the reductants and hence the sensor characteristics indicate an aspect of CO-junction chemistry not otherwise accessible *via* normal catalytic analysis. Even if catalytic effects are short range in nature,[47] the junction widths seen here by photo-STM are rather large, reflecting significant electronic–ionic depletion widths.[2] Not unexpectedly,[1] this interfacial trench has a steeper gradient on its Cu_2O side of the junction, but this might also reflect the fact that photoexcitation is easier in Cu_2O than ZnO (with a band-gap of 3.2 eV at 300 K) or that less effective Cu^+ transport occurs in cuprite than Zn^{2+} in wurtzite (despite its smaller ionic size).

Conclusions

CuO_x addition to ZnO_y can raise the selectivity of methanol synthesis and can induce a conductivity response to CO. These are inter-related phenomena which should be investigated in parallel. It is uncertain if the junction in the polycrystalline film was different (in that it can adsorb pyridine [Fig. 7(*b*)]) from the dispersed sample [Fig. 2(*b*)] which could not adsorb pyridine. Catalytic and sensor chemistry of CuO_x/ZnO_y are related[48] and should be simultaneously explored, optimised and exploited. Work on *in-situ* photo-STM is required in CO–air and CO–hydrogen atmospheres at operating temperatures and is now envisaged. It is hoped that photo-STM will in future see catalytic or sensor processes at such n/p micro-junctions[49] and that switching-on of these processes through a bias voltage[50] will ultimately be possible.

The authors thank the Royal Society for support of Y.W., the Paul Instrument Fund of the Royal Society for support for V.A.S., EPSRC for support for M.A.M.L. and CRLL for permitting the thin films to be prepared.

References

1 A. R. Frederickson and A. S. Karakashian, *J. Appl. Phys.*, 1995, **77**, 1627.
2 C. H. Townes, A. N. Holden, J. Bardeen and F. R. Merritt, *Phys. Rev.*, 1947, **71**, 644.
3 P. R. Fischer and G. L. Richmond, ACS Chicago, 1995, **210**, 063-COLL.
4 G. L. Richmond, J. M. Robinson and U. L. Shannon, *Prog. Surf. Sci.*, 1988, **28**, 1.
5 T. Seiyama and S. Kagawa, *Anal. Chem.*, 1966, **38**, 1069; T. Nenov and S. Yordanov, *Sens. Actuators B*, 1992, **8**, 117; S. T. Jun and G. M. Choi, *Sens. Actuators B*, 1994, **17**, 175.
6 A. R. Raju and C. N. R. Rao, *Sens. Actuators B*, 1991, **3**, 305; E. Traversa and A. Bearzotti, *J. Ceram. Soc. Jpn.*, 1995, **103**, 11; J. Muller and S. Weissenrieder, *Fresenius J. Anal. Chem.*, 1994, **349**, 380; V. V. Malyshev, A. A. Vasiliev, A. V. Eryshkin, E. A. Koltypin, Y. I. Shubin, A. I. Buturlin, V. A. Zaikin and G. B. Chakhunashvili, *Sens. Actuators B*, 1992, **10**, 11.
7 Q. J. Gu, Z. L. Ma, N. Liu, X. Ge, W. B. Zhao, Z. Q. Xue, S. J. Pang and Z. Y. Hua, *Surf. Sci.*, 1995, **327**, 241.
8 A. V. Chadwick, N. V. Russell, A. R. Whitham and A. Wilson, *Sens. Actuators B*, 1994, **18**, 99.

9 Y. Ushio, M. Miyayama and H. Yanagida, *Sens. Actuators B*, 1994, **17**, 221; *Jpn. J. Appl. Phys. I*, 1994, **33**, 1136.
10 Y. Nakamura, H. Yoshioka, M. Miyayama, H. Yanagida, T. Tsurutani and Y. Nakamura, *J. Electrochem. Soc*., 1990, **137**, 940.
11 P. Porta, M. C. Campa, G. Fierro, M. Lojacono, G. Minelli, G. Moretti and L. Stoppa, *J. Mater. Chem*., 1993, **3**, 505; J. Skrzypek, J. Sloczynski and S. Ledakowicz, *Methanol Synthesis*, Polish Scientific Publishers, 1994; J. C. Slaa, G. J. M. Weierink, J. G. Vanommen and J. R. H. Ross, *Catal. Today*, 1992, **12**, 481; J. C. Slaa, J. G. Vanommen and J. R. H. Ross, *Catal. Today*, 1992, **15**, 129; G. C. Chinchen, K. C. Waugh and D. A. Whan, *Appl. Catal*., 1986, **25**, 101; I. Boz, D. Chadwick, I. S. Metcalfe and K. Zheng, *Stud. Surf. Sci. Catal*., 1993, **75**, 2785; M. Bowker, H. Houghton, K. C. Waugh, T. Giddings and M. Green, *J. Catal*., 1983, **84**, 252; M. Bowker, *Vacuum*, 1983, **33**, 669; J. C. Amphlett, R. F. Mann, C. McKnight and R. D. Weir, *Proc. Intersoc. Energy Convers. Energy Conf*., 1985, **20**, 2772.
12 K. L. Siefering and G. L. Griffin, *Surf. Sci*., 1989, **207**, 525.
13 V. Bolis, B. Fubini, E. Giamello and A. Reller, *J. Chem. Soc., Faraday Trans. 1*, 1989, **85**, 855.
14 M. A. Vest, K. Lui and H. H. Kung, *J. Catal*., 1989, **120**, 231; G. M. Schwab and H. Seemueller, *Mem. Soc. Roy. Sci., Liege Collect*., 1971, **8**, 55; C. T. Au, W. Hirsch and W. Hirschwald, *Surf. Sci*., 1988, **199**, 507.
15 J. C. J. Bart and R. P. A. Sneeden, *Catal. Today*, 1987, **2**, 1.
16 H. S. Taylor and C. O. Strother, *J. Am. Chem. Soc*., 1934, **56**, 586; R. R. Gay, M. H. Nodine, V. E. Heinrich, H. J. Zeiger and E. I. Solomon, *J. Am. Chem. Soc*., 1980, **102**, 6752; G. L. Griffin and J. T. Yates, *J. Chem. Phys*., 1982, **77**, 3751.
17 E. Mollwo, G. Muller and P. Wagner, *Solid State Commun*., 1973, **13**, 1283; R. G. Herman, K. Klier, G. W. Simmons, B. P. Finn, J. B. Bulko and T. Kobylinski, *J. Catal*., 1979, **56**, 407; T. Arunarkavalli, G. U. Kulkarni and C. N. R. Rao, *Catal. Lett*., 1993, **20**, 259.
18 M. A. M. Luengo, P. A. Sermon, Y. Sun, M. S. W. Vong and V. A. Self, *Solid State Ionics*, 1997, in press.
19 R. A. Hadden, P. J. Lambert and C. Ranson, *Appl. Catal. A*, 1995, **122**, L1.
20 J. C. Frost, *Nature* (*London*), 1988, **334**, 577; R. Zhang, A. Ludviksson and C. T. Campbell, *Catal. Lett*., 1994, **25**, 277; G. J. Millar, C. H. Rochester and K. C. Waugh, *J. Chem. Soc., Faraday Trans. 1*, 1992, **88**, 2257, 3497.
21 J. E. Bailie, C. H. Rochester and G. J. Millar, *Catal. Lett*., 1995, **31**, 333.
22 M. S. W. Vong, M. A. Yates, P. Reyes, A. Perryman and P. A. Sermon, *Proc. 9th. Intern. Cong. Catal. The Chemical Institute of Canada, Ottawa*, ed. M. J. Philips and M. Ternan, pp. 545–552.
23 S. S. Fu and G. A. Somorjai, *Surf. Sci*., 1990, **237**, 87; S. V. Didziulis, K. D. Butcher, S. L. Cohen and E. I. Solomon, *J. Am. Chem. Soc*., 1989, **111**, 7110.
24 E. P. S. Barrett, G. C. Georgiades and P. A. Sermon, *Sens. Actuators B*, 1990, **1**, 116.
25 P. J. Moller, S. A. Komolov, E. F. Lazneva and E. H. Pedersen, *Surf. Sci*., 1995, **323**, 102.
26 G. S. Rohrer and D. A. Bonnell, *Surf. Sci*., 1991 **247**, L195; K. Itaya and E. Tomita, *Surf. Sci*., 1989, **219**, L515; A. B. Boffa, H. C. Galloway, P. W. Jacobs, J. J. Benitez, J. D. Batteas, M. Salmeron, A. T. Bell and G. A. Somorjai, *Surf. Sci*., 1995, **326**, 80.
27 V. A. Self and P. A. Sermon, *Rev. Sci. Instrum*., 1996, **67**, 2096.
28 S. R. Morrison, *Surf. Sci*., 1971, **27**, 586; 1975, **50**, 329.
29 A. L. Boyce, P. A. Sermon, M. S. W. Vong and M. A. Yates, *React. Kinet. Catal. Lett*., 1991, **44**, 309.
30 Y. Mizokawa and S. Nakamura, *Jpn. J. Appl. Phys*., 1977, **16**, 1073.
31 K. M. Sancier, *J. Phys. Chem*., 1972, **76**, 2527.
32 P. A. Sermon, M. A. Martin-Luengo and Y. Wang, *Proc. 10th Int. Congr. Catal. Hungary, Elsevier Sci*., ed. Guczi, F. Solymosi and P. Tetenyi, 1992, pp. 2773–2776.
33 J. J. Carberry, *J. Catal*., 1987, **107**, 248.
34 D. Stirling, F. S. Stone and M. S. Spencer, *Proc. 10th Int. Congr. Catal. Hungary, Elsevier Sci*., ed. Guczi, F. Solymosi and P. Tetenyi, 1992, p. 1507.
35 R. P. Eischens, W. A. Pliskin and S. A. Francis, *J. Chem. Phys*., 1954, **22**, 1786; R. P. Eischens and N. A. Pliskin, *Adv. Catal*., 1958, **10**, 2.
36 M. A. Martin-Luengo, P. A. Sermon and Y. Wang, *Stud. Surf. Sci. Catal*., 1993, **75C**, 2773.
37 H. H. Kung, *Catal. Rev*., 1980, **22**, 235; E. L. Muetterties and J. Stein, *Chem. Rev*., 1979, **79**, 479.
38 A. A. Tsyganenko, J. Lamotte, J. Saussey and J. C. Lavalley, *J. Chem. Soc., Faraday Trans. 1*, 1989, **85**, 2397.
39 C. T. Campbell, K. A. Daube and J. M. White, *Surf. Sci*., 1987, **182**, 458.
40 S. W. Gaarenstroom and N. Winograd, *J. Chem. Phys*., 1977, **67**, 3500.
41 J. F. Walsh, R. Davis, C. A. Muryn, G. Thornton, V. R. Dhanak and K. C. Prince, *Phys. Rev. B*, 1993, **48**, 14749.
42 J. A. Rodriguez and C. T. Campbell, *Surf. Sci*., 1988, **194**, 475.
43 J. C. Lavalley and R. T. J. Saussey, *6th. Sov. Fr. Seminar. Po. Katal. Sb. Dokl. M 97*, 1983; R. C. Baetzold, *J. Phys. Chem*., 1985, **89**, 4150.
44 R. Burch, R. J. Chappell and S. E. Golunski, *J. Chem. Soc., Faraday Trans. 1*, 1989, **85**, 3569; R. Burch and R. J. Chappell, *Appl. Catal*., 1988, **45**, 131; R. Burch, R. J. Chappell and S. E. Golunski, *Catal. Lett*., 1988, **1**, 439; M. J. Chung, D. J. Moon, H. S. Kim, K. Y. Park and S. K. Ihm, *J. Mol. Catal. A*, 1996, **113**, 507.
45 W. Schottky, *Naturwissenschaften*, 1938, **26**, 843.
46 E. Weiss and M. Folman, *J. Chem. Soc., Faraday Trans. 1*, 1986, **82**, 2025.
47 J. Pritchard, *Nature* (*London*) 1990, **343**, 592.
48 G. M. Schwab and R. Siegert, *Z. Phys. Chem*., 1966, **50**, 191.
49 M. Bartkowiak, G. D. Mahan, F. A. Modine and M. A. Alim, *Jpn. J. Appl. Phys. 2*, 1996, **35-4A**, 414; *J. Appl. Phys*., 1996, **79**, 273.
50 Y. Nakamura, K. Watanabe, S. J. Jung, H. Osawa, H. Yoshioka and H. Yanagida, *J. Catal*., 1995, **153**, 350; C. G. Vayenas, S. Bebelis and S. Ladas, *Nature* (*London*) 1990, **343**, 625.

Paper 7/00747G; *Received* 3*rd February*, 1997